Applied Catalysis B: Environmental 232 (2018) 108–116

Contents lists available at ScienceDirect

Applied Catalysis B: Environmental

journal homepage: www.elsevier.com/locate/apcatb

Quasi free K cations confined in hollandite-type tunnels for catalytic solid (catalyst)-solid (reactant) oxidation reactions

Taizheng Liu[a], Qian Li[a], Ying Xin[a], Zhaoliang Zhang[a,*], Xingfu Tang[b], Lirong Zheng[c], Pu-Xian Gao[d,*]

[a] School of Chemistry and Chemical Engineering, Shandong Provincial Key Laboratory of Fluorine Chemistry and Chemical Materials, University of Jinan, No. 336, West Road of Nan Xinzhuang, Jinan, 250022, PR China
[b] Shanghai Key Laboratory of Atmospheric Particle Pollution and Prevention (LAP3), Department of Environmental Science and Engineering, Fudan University, Shanghai, 200433, PR China
[c] Institute of High Energy Physics, Chinese Academy of Sciences, Beijing, 100049, PR China
[d] Nanomaterials Science Laboratory, Department of Materials Science and Engineering & Institute of Materials Science, University of Connecticut, 97 N. Eagleville Rd., Storrs, CT, 06269-3136, USA

ARTICLE INFO

Keywords:
Soot combustion
Cryptomelane
Potassium
Hollandite
Solid-solid reaction

ABSTRACT

Identification of catalytically active species and reaction pathway in catalytic solid (catalyst)-solid (reactant) reactions is a nontrivial task as exemplified in diesel soot oxidation (combustion), the technology for control of diesel particulate emissions. A physical contact between catalytically active species and solid soot is usually deemed necessary. Herein, thermally-stable hollandite-type α-MnO_2 ($K_xMn_8O_{16}$) nanorod catalysts have been synthesized with one-dimensional tunnel structures partially filled with relatively mobile K cations. These tunnel-confined quasi free K cations are revealed to be responsible for the catalytic soot oxidation activity, proving that physical contact between soot and K cations is unnecessary for solid-solid reaction. A novel catalyst, $K_yTi_8O_{16}$ has been successfully designed to boost the catalytic activity in TiO_2 toward soot oxidation by engineering a K-contained hollandite-type isostructure.

1. Introduction

The characterization and identification of catalytically active species are essential but nontrivial for understanding catalytic mechanism and designing advanced heterogeneous catalysts [1], which are particularly challenging when dealing with solid (catalyst) and solid (reactant) reaction systems due to their usually poor contact between each other [2–6]. For example, during catalytic diesel soot oxidation in gaseous O_2 (the technology for control of diesel particulate emissions), alkali metals such as potassium (K)-containing oxides are typical robust catalysts which are suggested to improve the physical contact bewteen soot and catalyst through free KO_x species and thus the catalytic activity [7,8]. On the other hand, a few work has proposed that K species confined in hollandite-type tunnel structures such as cryptomelane (2 × 2 edge-shared MnO_6 octahedral chains are corner connected to form a one-dimensional tunnel, which is partially filled with K cations) may help enhance the surface oxygen defects to improve soot oxidation activity [9,10]. It is unclear how these KO_x species exactly distribute and function although it is predicted that the K cations are partially filled and loosely bounded inside the tunnels [11–13] to create non-contact scenarios between soot and K cations. Such an intriguing possibility was raised in a striking enhancement of the catalytic activity observed in Rh particles encapsulated inside carbon nanotubes for the conversion of CO and H_2 to ethanol [14].

Mn-based oxides possess many applications in gaseous heterogeneous catalytic reactions for environmental applications [15], such as catalytic CO oxidation [16] and volatile organic compounds (VOCs) combustion [17]. Recently, Wasalathanthri et al investigated the potential of mesoporous Mn oxides in catalytic oxidation of diesel soot [18]. Transition metal (Co, Cu and Ni)-doped α-MnO_2 nanowires were also reported [19]. Specifically, Bueno-López and his colleagues have found that the cryptomelane is more active for soot combustion than all the commercially available pure manganese oxides, namely MnO, MnO_2, Mn_2O_3, Mn_3O_4, and natural MnO_2 [20–22]. Unfortunately, effects of the K concentration on the catalytic activity are still far from clear [23]. Even though the cryptomelane has been reported for catalytic combustion of VOCs, the effect of the amount of alkali doping to activity is controversial [11,13]. In this paper, the intrinsic activity for soot combustion on cryptomelanes with quasi free K cations confined in the tunnel ($K_xMn_8O_{16}$) shows a clear positive correlation with the K

* Corresponding authors.
E-mail addresses: chm_zhangzl@ujn.edu.cn (Z. Zhang), puxian.gao@uconn.edu (P.-X. Gao).

https://doi.org/10.1016/j.apcatb.2018.03.049
Received 27 August 2017; Received in revised form 15 March 2018; Accepted 16 March 2018
Available online 18 March 2018
0926-3373/

contents. This is the first direct experimental evidence for K cations being active species for soot oxidation. As a proof of concept, we demonstrated that TiO_2, a poor oxidation catalyst, can be greatly improved by using a hollandite-type iso-structure ($K_yTi_8O_{16}$). The K cations in tunnels serve as catalytically active species.

2. Experimental

2.1. Catalyst preparation

The catalysts were prepared by a solid phase method. The manganese carbonates ($MnCO_3$) and potassium methoxide (CH_3OK) were first ground in an agate mortar for 30 mins. The molar ratios of $MnCO_3$ and CH_3OK were 4:1, 4:1.1 and 4:1.2. The mixture was calcined in tube furnace at 620 °C for 12 h in air flow, and then the precursor powder was washed by deionized water to remove the surface K species completely [10,24–26], and then calcined again in tube furnace at 620 °C for 2 h in air flow. The catalysts obtained were named KMnO-10, KMnO-11 and KMnO-12, respectively. The Mn_2O_3 was obtained by calcining the $MnCO_3$ in tube furnace at 620 °C for 12 h in air.

The isostructural hollandite-type $K_yTi_8O_{16}$ were prepared by a solid phase method [27,28]. Typically, the mixture of K_2CO_3 and TiO_2 (anatase) was grinded in an agate mortar for 1 h, and then calcined at 1000 °C for 8 h under an 5% H_2/N_2 atmosphere. Therein, the molar ratios of K_2CO_3 and TiO_2 were 1:9 and 1:10. In order to remove the surface K species, the resultant specimens were treated by copious amount of deionized water under stirring for 24 h [10]. The final products were filtered and dried at 120 °C overnight. The catalysts obtained were named KTiO-1 and KTiO-2, respectively. For reference, the pure anatase TiO_2 was also calcined at 1000 °C for 8 h under an 5% H_2/N_2 atmosphere, which is denoted as reduced TiO_2.

2.2. Catalyst characterization

X-ray powder diffraction (XRD) patterns were recorded on a Rigaku D/max-rc diffractometer. Transmission electron microscopy (TEM) equipped with selected area electron diffraction (SAED) and energy dispersive spectroscopy (EDS) was conducted on a JEOL JEM-2010 microscope at an accelerating voltage of 200 kV. Surface area and pore size distribution were determined by N_2 adsorption/desorption at 77 K using Brunauer-Emmett-Teller (BET) method with a Micromeritics ASAP 2020 instrument after off gassing at 300 °C for 5 h prior to analysis. Inductively coupled plasma-atomic emission spectrometer (ICP–AES) experiments were carried out on an IRIS Intrepid IIXSP instrument from Thermo Elemental. X-ray absorption fine-structure (XAFS) measurements were performed on Beijing synchrotron radiation facility (BSRF, Beijing, China). IR experiments were carried out using a FTIR spectrometer (Bruker Tensor 27) over the range 400–4000 cm^{-1} with 32 scans at a resolution of 4 cm^{-1}. The samples were diluted with KBr in a ratio of 1:100. The temperature programmed reduction with H_2 (H_2–TPR) experiments were performed in a quartz reactor with a thermal conductivity detector (TCD) to monitor H_2 consumption. A 50 mg sample was pretreated in situ at 500 °C for 30 mins in a flow of O_2 (30 ml/min) and cooled to room temperature in the presence of O_2. After purging by N_2, TPR was conducted at 10 °C/min up to 600 °C in a 30 mL/min flow of 5 vol.% H_2 in N_2. To quantify the total amount of H_2 consumption, the CuO was used as a calibration reference. X-ray photoelectron spectroscopy (XPS) data were obtained on an AXIS-Ultra instrument from Kratos Analytical using monochromatic Al Kα radiation (225 W, 15 mA and 15 kV) and low-energy electron flooding for charge compensation. To compensate for surface charge effects, the binding energies were calibrated using the C 1 s hydrocarbon peak at 284.60 eV.

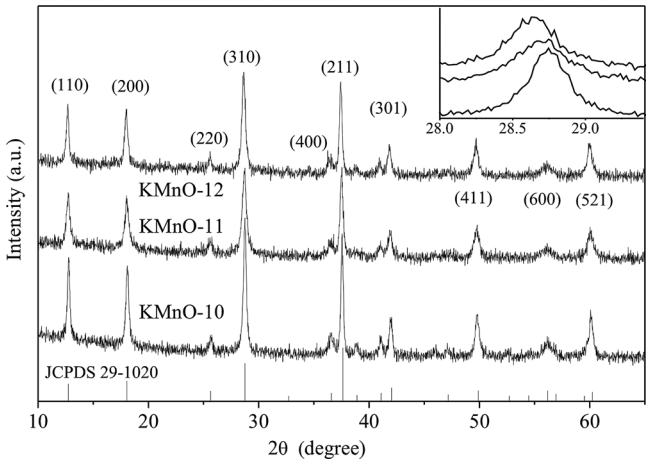

Fig. 1. XRD patterns of $K_xMn_8O_{16}$.

2.3. Activity measurement

Temperature-programmed oxidation (TPO) reactions were conducted in the fixed bed micro-reactor. Printex-U from Degussa is used as the model soot. The soot was mixed with the catalyst in a weight ratio of 1:9 in an agate mortar for 30 min, which results in a tight contact between soot and catalyst. While in loose contact conditions, the soot is mixed with the catalyst via shaking in a sample bottle for 24 h. A 50 mg sample of the soot/catalyst mixture was pretreated in a flow of He (100 mL/min) at 200 °C for 30 min to remove surface-adsorbed species. After cooling down to room temperature, a gas flow with 5 vol.% oxygen in He was introduced and then TPO was started at a heating rate of 5 °C/min until 620 °C. CO and CO_2 concentrations in the effluent gas were online monitored using a gas chromatograph (GC) (SP-6890, Shandong Lunan Ruihong Chemical Instrument Corporation, China) fitted with a methanator. The temperature of the maximum rate for soot oxidation is named T_m. The selectivity to CO_2 formation is defined as the percentage CO_2 outlet concentration divided by the sum of the CO_2 and CO outlet concentrations.

The CO oxidation experiments were performed in the fixed bed micro-reactor. A 50 mg sample of the catalyst was pretreated in a flow of He (100 mL/min) at 200 °C for 30 mins to remove surface-adsorbed species. After cooling down to room temperature, a gas flow with 5 vol. % O_2 and 500 ppm CO in He (100 ml/min) was introduced and then TPO was started at a heating rate of 5 °C/min until 620 °C. CO and CO_2 concentrations in the effluent gas were online monitored using a gas chromatograph (GC) (SP-6890, Shandong Lunan Ruihong Chemical Instrument Corporation, China) fitted with a methanator. The conversion of CO was defined as the percentage CO_2 outlet concentration divided by the CO enterance concentrations.

The isothermal reactions were performed at 270 and 290 °C for $K_xMn_8O_{16}$ and $K_yTi_8O_{16}$ respectively, at which, a stable and low soot conversion (< 15%) was achieved in a kinetic regime [29]. The reaction rate for soot combustion is obtained from the slope of the conversion lines with time. Specific rates normalized by BET surface areas were used to characterize the intrinsic activity for soot combustion.

Isotopic isothermal reaction was performed by switching the flowing gas from 1% $^{16}O_2$ to 1% $^{18}O_2$ diluted in Ar at 340 °C. 50 mg of a mixture of the soot and catalyst in tight contact mode was employed. The effluent gas from the reactor was continuously monitored by a MS for all of the isotopic molecules of CO_2 (at m/z = 44, 46 and 48) [30].

3. Results and discussion

$K_xMn_8O_{16}$ nanorods were prepared by solid-phase reactions between $MnCO_3$ and CH_3OK at 620 °C. To ensure the absence of the surface K species, the as-prepared $K_xMn_8O_{16}$ nanorods were further

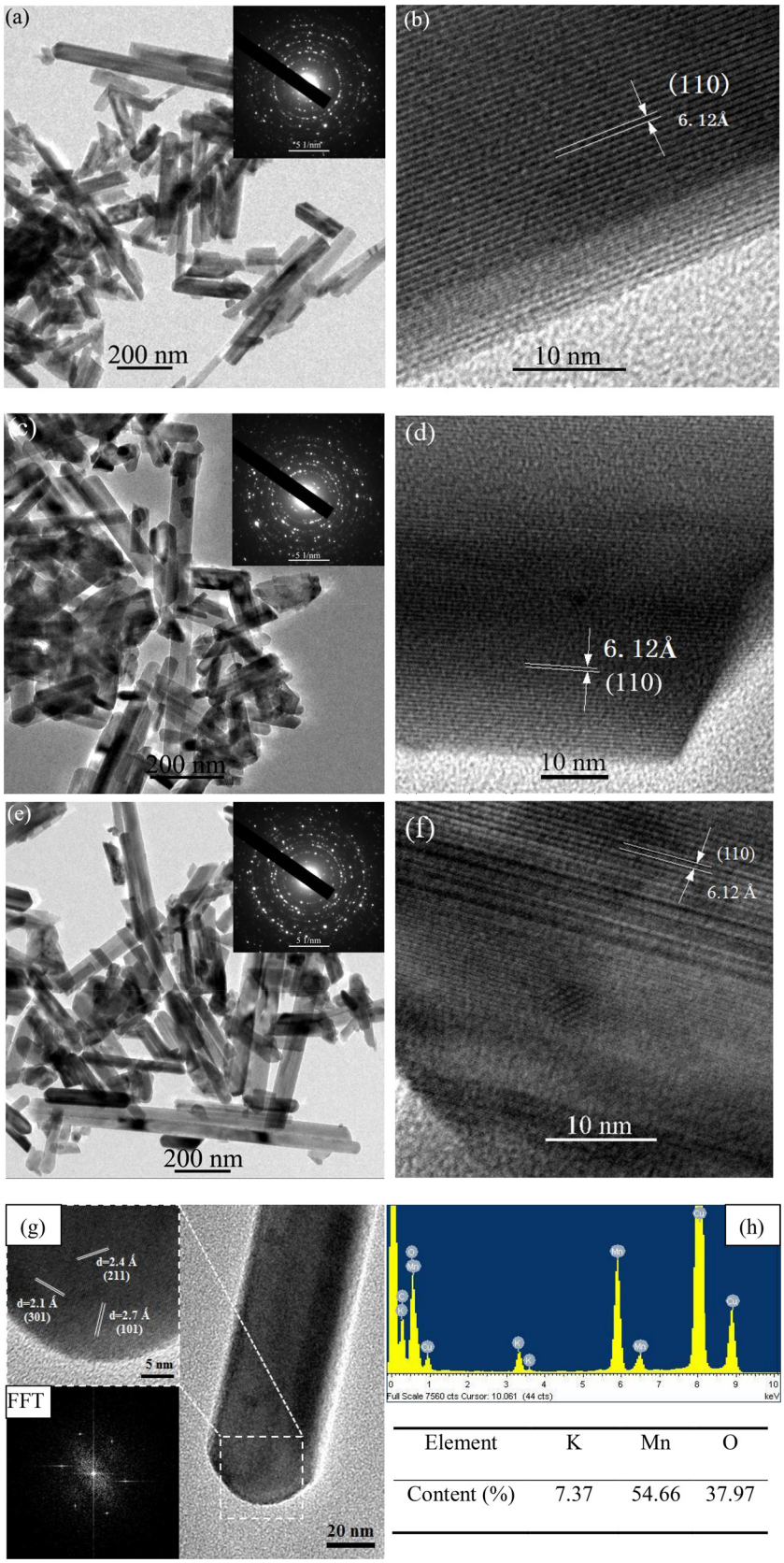

Element	K	Mn	O
Content (%)	7.37	54.66	37.97

Fig. 2. TEM characterizations for KMnO-10 (a and b), KMnO-11 (c and d) and KMnO-12 (e, f and g). EDS analysis of KMnO-12 (h).

washed by deionized water and recalcined at 620 °C for 2 h [10,24,25]. Li et al demonstrated that the surface K cations can be easily washed away using water [26]. XRD patterns confirm the cryptomelane structure of $K_xMn_8O_{16}$ ($x \leq 2$) (JCPDS 29-1020) nanorods (Fig. 1), although the relative intensities do not exactly match the standard pattern due to the anisotropic growth of nanorods along the [101] axis

Table 1
Physicochemical properties and specific rates normalized by BET surface areas at 270 °C.

Sample	K contents (wt.%)	K/Mn atomic ratio		Surface areas ($m^2 g^{-1}$)	Specific rates[a]	T_{max} (°C)	AOS[b]
		ICP	XPS				
KMnO-10	6.7	0.18	0.26	14.2	0.322	423	3.8/3.5
KMnO-11	7.1	0.20	0.27	16.0	0.458	417	3.9/3.6
KMnO-12	7.8	0.22	0.30	12.2	0.505	407	3.9/3.5

[a] $(mol\ s^{-1} m^{-2}) \times 10^{-8}$.
[b] From H_2-TPR/XPS.

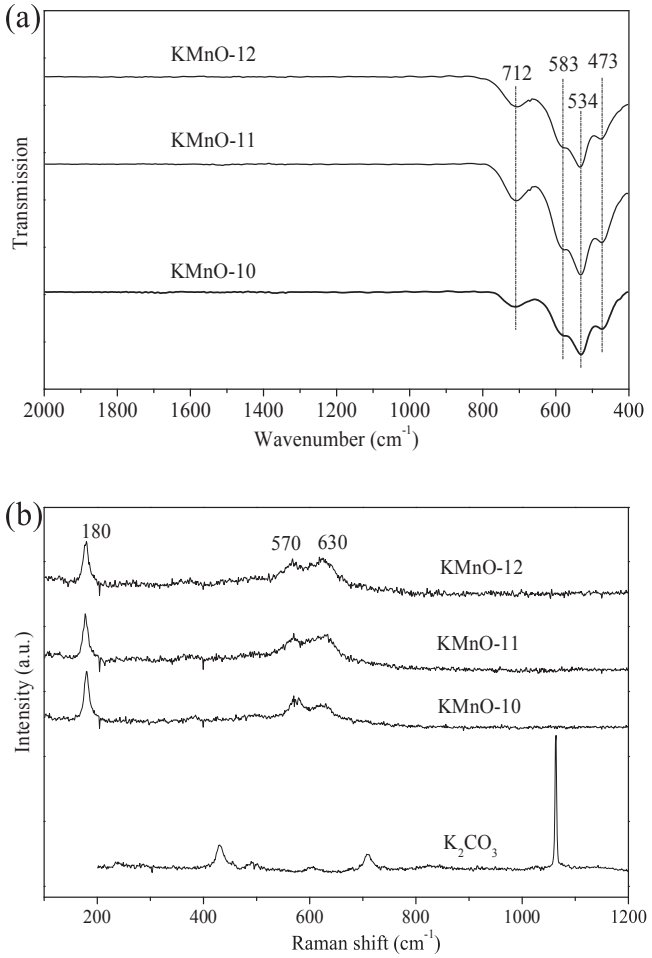

Fig. 3. IR (a) and Raman (b) spectra of KMnO-1, KMnO-11 and KMnO-12.

(Fig. 2a–g). However, the increase in the initial CH_3OK amount shifts the diffraction peaks to lower angles (Fig. 1 inset and Table 1), as a result of the successful incorporation of the mobilized K into cryptomelane tunnels. This allows us to determine the catalytically active species for catalytic soot oxidation normally occuring below 600 °C. ICP–AES shows the K contents of KMnO-10, KMnO-11 and KMnO-12 (Table 1), in coincidence with molecular formulas of $K_{1.4}Mn_8O_{16}$, $K_{1.5}Mn_8O_{16}$ and $K_{1.7}Mn_8O_{16}$, respectively. EDS analysis confirmed the K content for KMnO-12 (Fig. 2h).

Surface-sensitive IR (Fig. 3a) and Raman spectra (Fig. 3b) involve mainly vibrations of the octahedral MnO_6 skeleton and do not display a significant contribution from K cations in the channel [31–33]. As shown in Fig. 3, the IR vibrational mode of the Mn–O bonds in a cryptomelane structure appears in the region 400–800 cm^{-1} [31]. Similarly, only characteristic Raman peaks of Mn–O lattice vibrations were detected at 180, 570 and 630 cm^{-1} [32,33]. No spectral feature

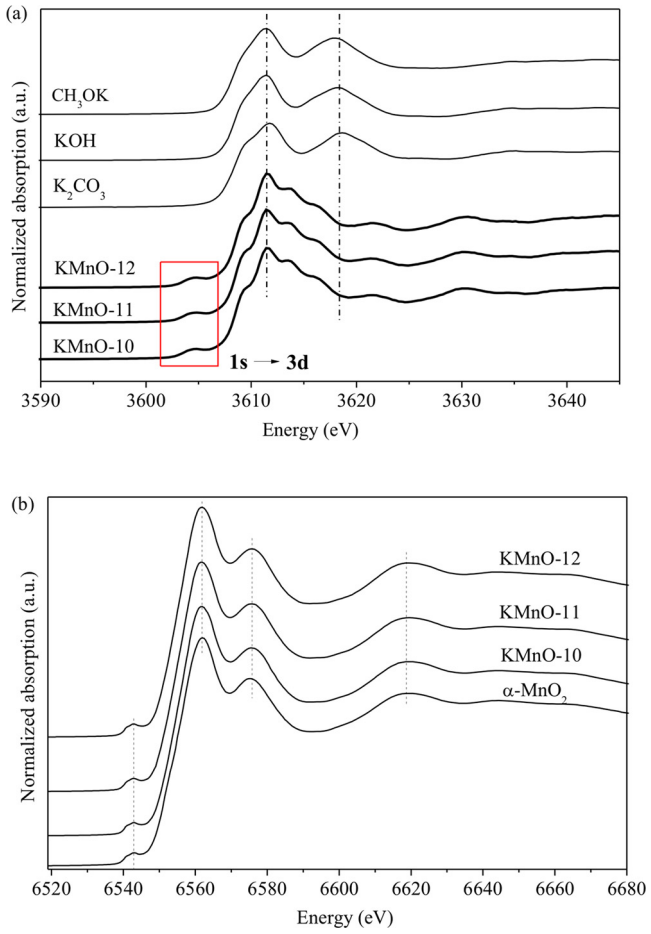

Fig. 4. Normalized absorption of K K-edge (a) and Mn K-edge (b) for $K_xMn_8O_{16}$ and standard samples.

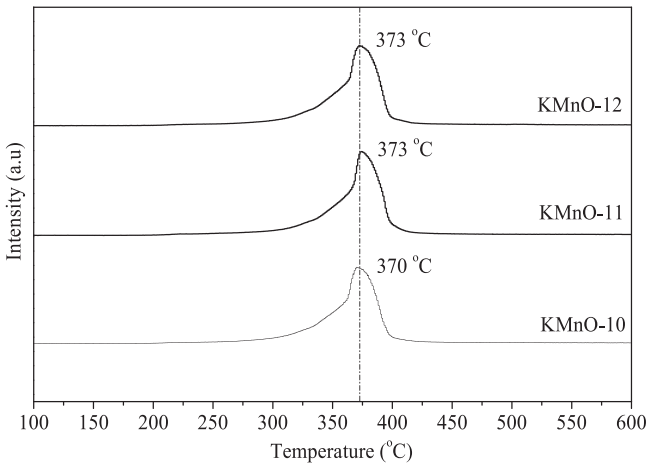

Fig. 5. H_2-TPR spectra for KMnO-10, KMnO-11 and KMnO-12.

was observed belonging to K species from both IR and Raman spectra, further confirming the absence of surface K species such as K carbonates.

The local bonding conditions were characterized by XANES (Fig. 4). The K K-edge XANES spectra for KMnO-10, KMnO-11 and KMnO-12 are identical to each other (Fig. 4a). However they are totally different from those of CH_3OK, KOH and K_2CO_3 as references. This confirmed that the K cations are bounded in the tunnel of cryptomelane. Likewise, the Mn K-edge XANES spectra are similar for KMnO-10, KMnO-11 and KMnO-12 to α-MnO_2 (Fig. 4b), suggesting that different K incorporation

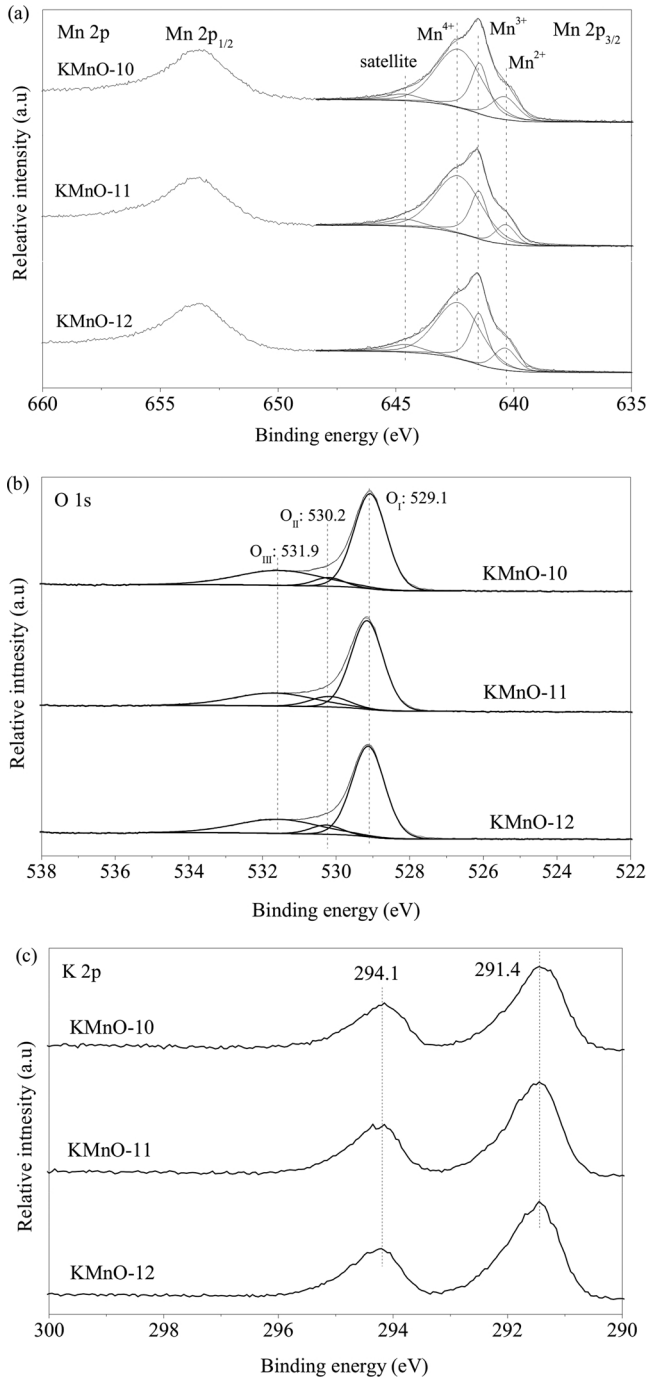

Fig. 6. Mn 2p (a), O 1 s (b) and K 2p (c) XPS spectra for KMnO-10, KMnO-11 and KMnO-12.

Table 2
Mn and O XPS data for KMnO-10, KMnO-11 and KMnO-12.

Samples	Mn^{2+}/O_I		Mn^{3+}/O_{II}		Mn^{4+}/O_{III}		AOS
	Position (eV)	Area (%)	Position (eV)	Area (%)	Position (eV)	Area (%)	
KMnO-10	640.40/ 529.1	13.7/ 67.11	641.45/ 530.2	25.7/5.55	642.33/ 531.9	60.6/ 27.33	3.5
KMnO-11	640.36/ 529.1	9.7/ 66.53	641.48/ 530.2	26.4/9.35	642.35/ 531.9	63.9/ 24.12	3.6
KMnO-12	640.36/ 529.1	12.0/ 67.26	641.48/ 530.2	27.9/6.48	642.35/ 531.9	60.1/ 26.26	3.5

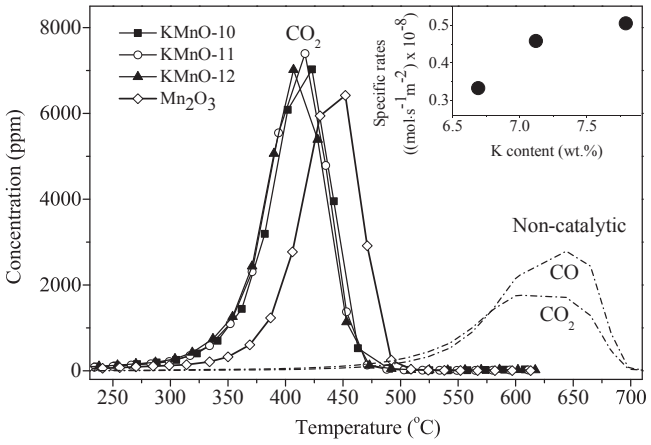

Fig. 7. TPO patterns for soot combustion with O_2 on $K_xMn_8O_{16}$ under tight contact conditions. Inset: The relationship between specific rates and K contents.

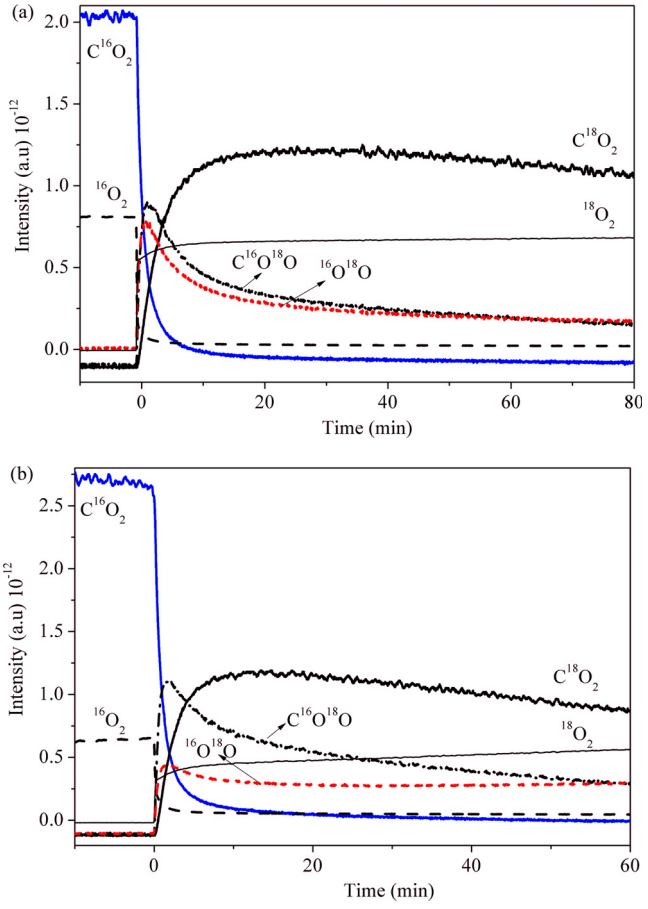

Fig. 8. The isothermal reaction for soot combustion at 340 °C after 1% $^{16}O_2$ was switched to 1% $^{18}O_2$ in He on KMnO-10 (a) and KMnO-12 (b).

contents do not influence the basic structure of MnO_6 octahedra molecular sieve (OMS-2). In other words, there is only a weak interaction between K and Mn, which results in a high mobility of K cations in the tunnels (quasi free K cations). This is in agreement with IR and Raman results, which show the absence of Mn–K chemical bonds [31–33].

The weak interaction between Mn and K was further demonstrated by H_2–TPR (Fig. 5). The reduction profiles are characterized by asymmetrical peaks centered at 370 ± 3 °C. For the three samples, the peak positions essentially do not change with the K content, suggesting that the introduction of different K contents does no influence the reducibility property of Mn. Furthermore, the reduction peak is assigned

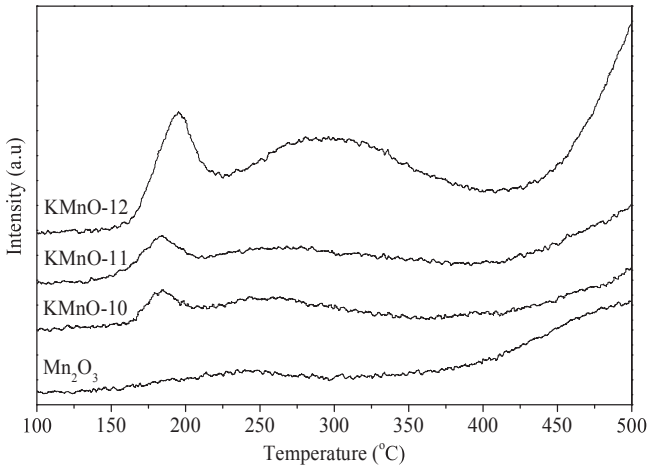

Fig. 9. O_2-TPD spectra for Mn_2O_3, KMO-10, KMO-11 and KMO-12.

Table 3
Physicochemical properties and reaction rates at 290 °C.

Sample	K contents (wt.%)	K/Ti atomic ratio		Reaction rates (μmol min^{-1})	T_{max} (°C)	Ti^{3+}/Ti^{4+} from XPS
		ICP	XPS			
KTiO-1	5.3	0.13	0.4	0.09	511	0.23
KTiO-2	6.2	0.15	0.5	0.68	460	0.29

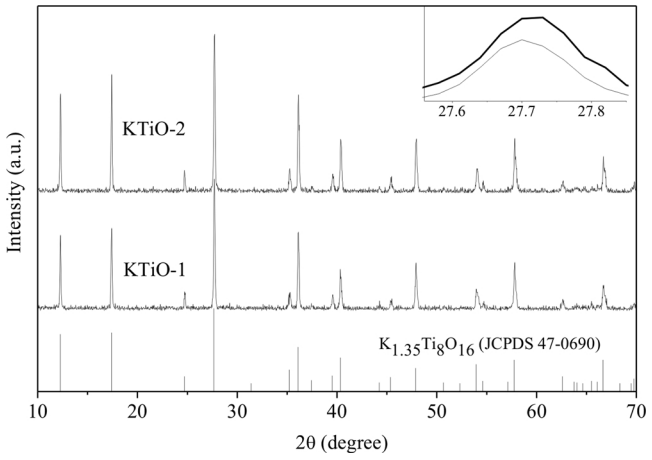

Fig. 10. XRD patterns of KTiO-1 and KTiO-2.

to the stepwise reduction of MnO_2 to Mn_2O_3, Mn_3O_4 and MnO [34]. The average oxidation state (AOS) of Mn in the bulk was calculated from the total consumption of H_2 from 100 to 500 °C, assuming MnO the final state. The obtained AOS values for KMnO-10, KMnO-11 and KMnO-12 (Table 1) appeared to be very close to the literature report value (~3.8) [35,36]. Therefore, the modulation of the K content in the cryptomelane structure does not have a significant effect on AOS and reducibility, as indicated by the similar CO oxidation activity (Fig. S1), because the surface lattice oxygen is responsible for the low temperature CO oxidation [37].

The detailed valences of Mn, O and K were characterized by XPS (Fig. 6 and Table 2). The Mn $2p_{3/2}$ spectra of KMnO-10, KMnO-11 and KMnO-12 are deconvoluted into three peaks attributed to Mn^{2+}, Mn^{3+} and Mn^{4+}, respectively (Fig. 6a) [13,38]. The AOS of Mn from XPS (Table 2) is lower than that in bulk from H_2-TPR (Table 1), suggesting the existence of oxygen vacancies on the surface. The O 1 s spectra show three kinds of oxygen species, bulk lattice oxygen O^{2-} (O_I), surface lattice oxygen O^{2-} (O_{II}) and surface adsorbed O_2^- and O^- (O_{III}), respectively (Fig. 6b) [39,40]. The areas of the latter two peaks are nearly the same, suggesting that the active oxygen amounts are not affected by K contents either. However, the binding energy of K 2p at 294.1 eV ($2p_{1/2}$) and 291.4 eV ($2p_{3/2}$) (Fig. 6c) is lower than that of bulk K_2CO_3 and surface-surported K on ZrO_2 and MgO (295.6 and 292.9 eV, respectively) [41], suggesting the electron density of the confined K cations in the tunnel increased in comparison with the free K cations [42]. Possibly, the K valence in cryptomelane is lower than + 1, which should play a pivotal role in the redox cycle including the O_2 dissociation.

The activity for soot combustion was first evaluated by TPO reactions (Fig. 7). All the three $K_xMn_8O_{16}$ samples displayed better activity than Mn_2O_3, which was obtained by calcining $MnCO_3$ without CH_3OK. The water-washed samples showed almost the same activity as the fresh ones (Fig. S2), suggesting that the K^+ ions in the tunnel of cryptomelane are stable in the water-containing atmosphere. As an example, no change for K contents was detected by ICP analysis on water-washed KMnO-10. This may be related to the excellent hydrophobicity for cryptomelane [43]. The T_m decreases in the sequence of KMnO-10 < KMnO-11 < KMnO-12. Similar situation is obtained with O_2 under loose contact conditions between catalyst and soot mimicing the real situation in diesel exhaust (Fig. S3). Furthermore, the selectivity to CO_2 is nearly 100%, much higher than those of the K-supported catalysts on inert oxides such as ZrO_2, MgO, TiO_2 and SiO_2 [10,41]. The enhanced effect of selectivity to CO_2 could be attributed to the good activity of manganese oxides for CO oxidation (Fig. S1) [44]. Similar to activity results based on T_m, the intrinsic activity, namely, the specific rates normalized by BET surface areas for KMnO-10, KMnO-11 and KMnO-12 shows a same tendency (Table 1). Strikingly, the K contents nearly correlate linearly with the specific rates (Fig. 7 inset), confirming the quasi free K cations confined in the tunnels were active species for soot oxidation. To study the durability, the TPO experiments with O_2 on KMnO-12 under loose contact conditions between catalyst and soot were carried out for 5 cycles. As observed in Fig. S4, the T_m is nearly retained, indicating good reproducibility on repeated usage. After all reactions, the $K_xMn_8O_{16}$ catalysts are stable as demonstrated by Fig. S5.

The origin of the active oxygen species was determined using isotopic isothermal oxidation by taking KMnO-10 (Fig. 8a) and KMO-12 (Fig. 8b) as examples. Before switching from $^{16}O_2$ to $^{18}O_2$ (the left of zero), the main product was $C^{16}O_2$, confirming that the stable soot oxidation occurs. After switching from $^{16}O_2$ to $^{18}O_2$ (the right of zero), the concentration of $C^{16}O_2$ decreased gradually to zero due to the depletion of $^{16}O_2$ in gaseous phase. Comparatively, the production of $C^{16}O^{18}O$ and $^{16}O^{18}O$ increases and then decrease to zero after a maximum, while the $C^{18}O_2$ production monotonically increases and gets close to equilibrium with a decrease trend gradually due to the depletion of soot. This indicates that the gaseous oxygen has been activated by $K_xMn_8O_{16}$ and then is used to oxidize the soot. In addition, the desorption of $^{16}O^{18}O$ is detected, which also suggests the chemisorption [8] and activation of gaseous O_2 into surface adsorbed oxygen, as observed by O_2–TPD for Mn_2O_3, KMO-10, KMO-11 and KMO-12 (Fig. 9). Mn_2O_3 shows negligible oxygen desorption at low temperature. However, introduction of K results in the oxygen desorption from 150 °C. Furthermore, the desorbed oxygen increased with the increase in K contents, confirming the role of K species in activation of gaseous oxygen (Fig. 9).

Following above strategy, another isostructural hollandite $K_yTi_8O_{16}$ catalyst comprising double chains of TiO_6 octahedra forming (2 × 2) tunnels was prepared for soot combustion (Table 3). XRD patterns show that both KTiO-1 and KTiO-2 are indexed to the $K_{1.35}Ti_8O_{16}$ structure (JCPDS 47-0690) (Fig. 10) [45]. The diffraction peaks of KTiO-2 which contains more K content shift to higher angles than those of KTiO-1 (Fig. 10 inset), suggesting the encapsulation of K into tunnels [28]. The K K-edge XANES spectra are similar to those for $K_xMn_8O_{16}$, suggesting the similar environment of K cations in the tunnel of $K_yTi_8O_{16}$

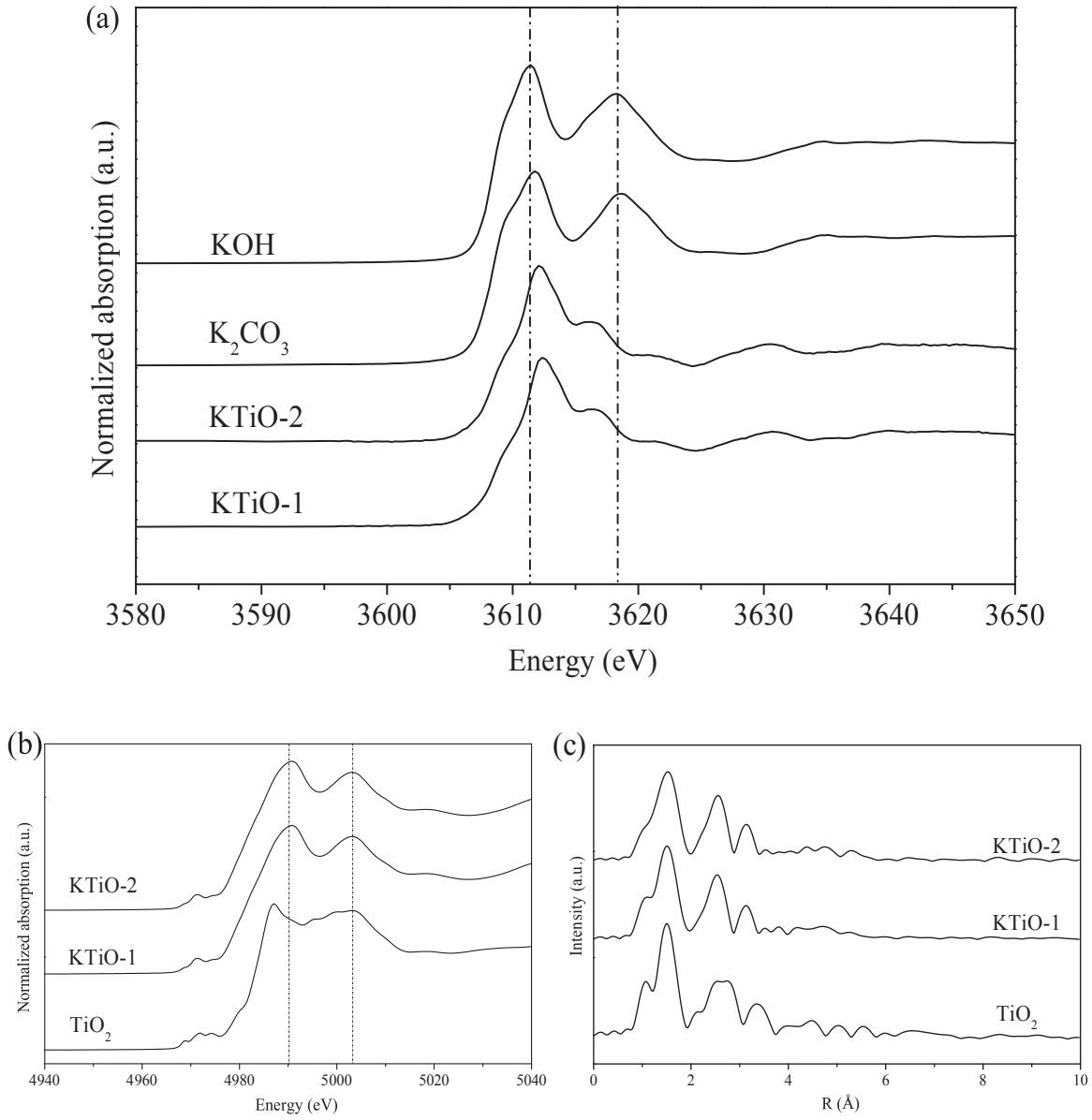

Fig. 11. Normalized absorption of K K-edge (a) and Ti K-edge (b) for KTiO-1, KTiO-2 and references. (c) Fourier transform of extended X-ray absorption fine structure (EXAFS) spectra near Ti K-edge for KTiO-1, KTiO-2 and TiO_2.

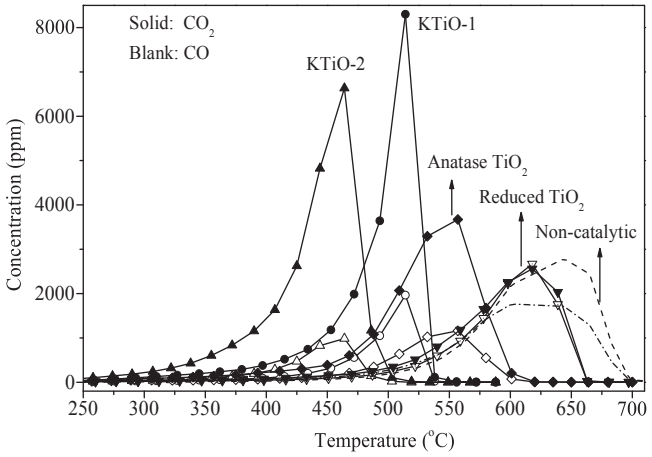

Fig. 12. TPO patterns for soot combustion with O_2 on KTiO-1, KTiO-2, TiO_2 and reduced TiO_2.

(Fig. 11a). However, the Ti K-edge spectra of KTiO-1 and KTiO-2 are different from that of TiO_2 (Fig. 11b and c), suggesting the strong interaction of K cations with TiO_2.

As expected, both activity and the selectivity to CO_2 increase in the sequence of KTiO-2 > KTiO-1 > anatase TiO_2 > reduced TiO_2 (Fig. 12), suggesting that the activity of $K_yTi_8O_{16}$ was closely related with K^+ ions in tunnels. The reduction of TiO_2 in H_2 will lead to excessive oxygen vacancies, which can induce the formation of less active species (like O^{2-}) rather than O_2^- and therefore decrease the activity of TiO_2 [46]. The reaction rates confirmed that the higher K contents the higher activity (Table 3). However, the comparatively low selectivity to CO_2 with respect to $K_xMn_8O_{16}$ is due to especially low activity of Ti oxides for CO oxidation (Fig. S6). Considering Ti oxides are much more inert than Mn oxides for thermal oxidation reactions, the improved activity of $K_yTi_8O_{16}$ again confirmed the confined K cations in the tunnels being active species. After TPO reactions, the structure of $K_yTi_8O_{16}$ is stable (Fig. S7).

In comparison with $K_xMn_8O_{16}$, $K_yTi_8O_{16}$ shows lower activity (higher T_m), which is correlated with the freedom of K cations confined

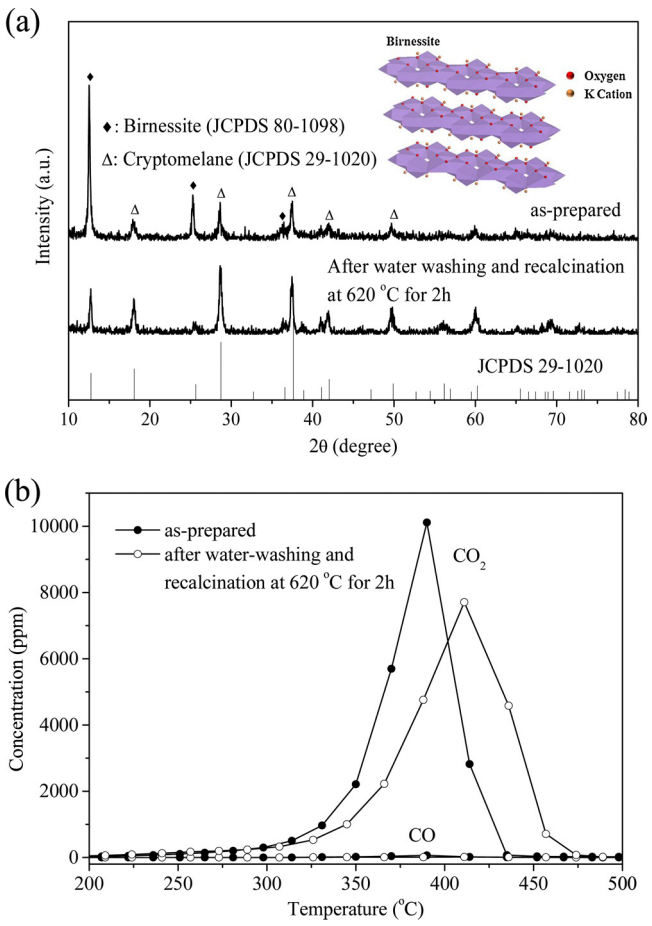

Fig. 13. XRD patterns (a) and TPO profiles (b) for the as-prepared KMnO-15 and after water-washing and recalcination at 620 °C for 2 h in air. Inset: schematic illustration of the birnessite structure.

in the tunnel. As indicated above, the interaction of K with Mn is much weaker than that with Ti, meaning that K cations in the former case are freer than in the latter case, in other word, a more stable salt ($K_yTi_8O_{16}$) was formed between K and TiO_2. However, it is acknowledged that only comparably free K cations are much active for soot combustion [8,10,41,47]. As discussed above, the role of active K species lies in the activation of gaseous O_2 into surface adsorbed oxygen. The latest finding shows the existence of the *d-sp* orbital hybridization of K ions in $K_xMn_8O_{16}$, i.e., the local transfer of *sp* electrons to empty *d* shell [48,49]. The K^+ *d-sp* hybridizations may originate from the electron transfer from O sp^3 orbitals with lone-pair electrons [42] to unoccupied K^+ *d-sp* frontier orbitals, resulting in electron-rich K atoms, analogue to metallic K atoms with the outermost hybridized orbitals [50], which leads to the feasible electron transfer from K to gaseous O_2, and thus oxygen activation. This coincides with the K 2p XPS analysis. On Mn-based hollandite oxides, the low-intensity pre-edge of the K centers with a pseudo-tetragonal prism structure was observed (Fig. 4), which confirmed the presence of 1*s*-3*d* dipole allowed contribution [40] due to *d-sp* hybridization; however, the same 1*s*-3*d* pre-edge feature is absent on the Ti-based counterparts (Fig. 11a), which is derived from the strong interaction between K and TiO_2. Combined with the isotopic trace results, the solid (soot reactant)-solid (hollandite-type K-containing oxide catalysts) oxidation reactions may follow an equivalent Eley-Rideal mechanism to the gas (reactant)-solid (catalyst)-gas (reactant) counterparts as for CO oxidation [51].

It is the electron effect that results in un-necessity for the contact between reactant soot and catalytic active K cations, similar to Zn^+ ions confined in ZSM-5 for CO oxidation [51]. Kotarba and co-authors found that the bulk K is much more effective than the surface K for soot oxidation, and explained that the latter increased activated oxygen recombination rate [52–56]. The catalytic role of K ions in layered TiO_2 ($K_2Ti_2O_5$) was also reported by Wang and coauthors [57,58]. However, the activity decreased after water-washing as in the case of birnessite (JCPDS 80-1098), therein K is located between the layers of MnO_2, where it is equivalently unstable as surface K species (Fig. 13). As shown in Fig. 13a, the layer-type birnessite phase (Fig. 13a inset) is dominant for the as-prepared KMnO-15 (the molar ratio of $MnCO_3$ and CH_3OK is 4:1.5). After water washing and re-calcination at 620 °C for 2 h, most of the layer-type birnessite would transform into the hollandite-type cryptomelane due to the dissolution of layered K cations during water washing (Fig. 13a). For the water-washed and recalcined KMnO-15, the activity correspondingly decreased in comparison with the as-prepared KMnO-15 (Fig. 13b).

As observed in ^{18}O isotopic experiments (Fig. 8) and our previous work [30], only meeting soot during desorption can the activated oxygen produce the product containing carbon. That is, the contact between soot and activated oxygen is foremost important, while the K cation can activate oxygen whether it contacts or not with soot. The similar finding was also reported on K^+ ion-exchanged ZSM-5 for soot combustion [59]. This understanding of the electron effect of K cations on soot oxidation could, in principle, allow a feasible design and discovery of various hydro-resistant K-containing catalysts through confining K in pores with dimension smaller than water molecule [60,61], like K-sodalite [62–64], K-glass [65–67], and other similarly structured materials.

4. Conclusions

The quasi free K cations confined in the one-dimensional tunnel structure of cryptomelane ($K_xMn_8O_{16}$) have been designed to eliminate the direct physical contact between soot and K cations for soot combustion. By correlating K contents with catalytic activity measurements, these K cations were confirmed to be the most active species in this catalyst system, while Mn cations promoted the oxidation of CO intermediate into the product CO_2. Another similar tunnel-structured $K_yTi_8O_{16}$ was successfully demonstrated with significantly boosted soot oxidation activity through engineering of K-contained hollandite structures. This provides a design and discovery principle of novel catalysts through identifying and engineering active species in a heterogeneous catalyst system. This strategy not only paves a path to develop high-activity and hydro-resistant soot combustion catalysts, but also has general applicability to other catalytic systems.

Acknowledgements

This work was supported by National Natural Science Foundation of China (No. 21477046), Key Technology R&D Program of Shandong Province (No. 2016ZDJS11A03) and the U.S. National Science Foundation under Award No. CBET-1344792.

Appendix A. Supplementary data

Supplementary material related to this article can be found, in the online version, at doi:https://doi.org/10.1016/j.apcatb.2018.03.049.

References

[1] M. Yang, S. Li, Y. Wang, J.A. Herron, Y. Xu, L.F. Allard, S. Lee, J. Huang, M. Mavrikakis, M. Flytzani-Stephanopoulos, Science 346 (2014) 1498–1501.
[2] A. Bueno-López, Appl. Catal. B: Environ. 146 (2014) 1–11.
[3] D. Fino, S. Bensaid, M. Piumetti, N. Russo, Appl. Catal. A: Gen. 509 (2016) 75–96.
[4] S. Liu, X. Wu, H. Luo, D. Weng, R. Ran, J. Phys. Chem. C 119 (2015) 17218–17227.
[5] Y. Wei, J. Liu, Z. Zhao, Y. Chen, C. Xu, A. Duan, G. Jiang, H. He, Angew. Chem. Int. Ed. 50 (2011) 2326–2329.
[6] E. Aneggi, D. Wiater, C. de Leitenburg, J. Llorca, A. Trovarelli, ACS Catal. 4 (2014)

172–181.
[7] H. An, C. Kilroy, P.J. McGinn, Catal. Today 98 (2004) 423–429.
[8] E. Aneggi, C. de Leitenburg, G. Dolcetti, A. Trovarelli, Catal. Today 136 (2008) 3–10.
[9] X. Yu, Z. Zhao, Y. Wei, J. Liu, Sci. Rep. 7 (2017) 43894.
[10] Q. Li, X. Wang, H. Chen, Y. Xin, G. Tian, C. Lu, Z. Zhang, L. Zheng, L. Zheng, Catal. Today 264 (2016) 171–179.
[11] V.P. Santos, O.S.G.P. Soares, J.J.W. Bakker, M.F.R. Pereira, J.J.M. Órfão, J. Gascon, F. Kapteijn, J.L. Figueiredo, J. Catal. 293 (2012) 165–174.
[12] J. Luo, Q. Zhang, J. Garcia-Martinez, S.L. Suib, J. Am. Chem. Soc. 130 (2008) 3198–3207.
[13] J. Hou, L. Liu, Y. Li, M. Mao, H. Lv, X. Zhao, Environ. Sci. Technol. 47 (2013) 13730–13736.
[14] X. Pan, Z. Fan, W. Chen, Y. Ding, H. Luo, X. Bao, Nat. Mater. 6 (2007) 507–511.
[15] H. Xu, N. Yan, Z. Qu, W. Liu, J. Mei, W. Huang, S. Zhao, Environ. Sci. Technol. 51 (2017) 8879–8892.
[16] V.P. Santos, S.A.C. Carabineiro, J.J.W. Bakker, O.S.G.P. Soares, X. Chen, M.F.R. Pereira, J.J.M. Órfão, J.L. Figueiredo, J. Gascon, F. Kapteijn, J. Catal. 309 (2014) 58–65.
[17] S.S.T. Bastos, S.A.C. Carabineiro, J.J.M. Órfão, M.F.R. Pereira, J.J. Delgado, J.L. Figueiredo, Catal. Today 180 (2012) 148–154.
[18] N.D. Wasalathanthri, T.M. SantaMaria, D.A. Kriz, S.L. Dissanayake, C.-H. Kuo, S. Biswas, S.L. Suib, Appl. Catal. B: Environ. 201 (2017) 543–551.
[19] D. Jampaiah, V.K. Velisoju, P. Venkataswamy, V.E. Coyle, A. Nafady, B.M. Reddy, S.K. Bhargava, ACS Appl. Mater. Interfaces 9 (2017) 32652–32666.
[20] I. Atribak, A. Bueno-López, A. García-García, P. Navarro, D. Frías, M. Montes, Appl. Catal. B: Environ. 93 (2010) 267–273.
[21] M.E. Becerra, N.P. Arias, O.H. Giraldo, F.E. López Suárez, M.J. Illán Gómez, A. Bueno López, Appl. Catal. B: Environ. 102 (2011) 260–266.
[22] M.E. Becerra, N.P. Arias, O.H. Giraldo, F.E. López Suárez, M.J. Illán Gómez, A. Bueno López, Catalysts 2 (2012) 352–367.
[23] J. Gao, C. Jia, L. Zhang, H. Wang, Y. Yang, S.F. Hung, Y.Y. Hsu, B. Liu, J. Catal. 341 (2016) 82–90.
[24] W. Kaspera, S. Zieliński, A. Kotarba, Catal. Commun. 98 (2017) 76–80.
[25] R. Kimura, J. Wakabayashi, S.P. Elangovan, M. Ogura, T. Okubo, J. Am. Chem. Soc. 130 (2008) 12844–12845.
[26] K. Li, J. Chen, Y. Peng, W. Lin, T. Yan, J. Li, J. Mater. Chem. A 5 (2017) 20911–20921.
[27] M. Sakao, N. Kijima, J. Akimoto, T. Okutani, Solid State Ion. 225 (2012) 502–505.
[28] L.D. Noailles, C.S. Johnson, J.T. Vaughey, M.M. Thackeray, J. Power Sources 81–82 (1999) 259–263.
[29] Z. Zhang, D. Han, S. Wei, Y. Zhang, J. Catal. 276 (2010) 16–23.
[30] G. Tian, H. Chen, C. Lu, Y. Xin, Q. Li, J.A. Anderson, Z. Zhang, Catal. Sci. Technol. 6 (2016) 4511–4515.
[31] C.M. Julien, M. Massot, C. Poinsignon, Spectrochim. Acta Part A 60 (2004) 689–700.
[32] T. Gao, M. Glerap, F. Krumeich, R. Nesper, H. Fjellvåg, P. Norby, J. Phys. Chem. C 112 (2008) 13134–13140.
[33] J. Hou, Y. Li, L. Liu, L. Ren, X. Zhao, J. Mater. Chem. A 1 (2013) 6736.
[34] X. Tang, J. Li, L. Sun, J. Hao, Appl. Catal. B: Environ. 99 (2010) 156–162.
[35] K. Malinger, Y. Ding, S. Sithambaram, L. Espinal, S. Gomez, S. Suib, J. Catal. 239 (2006) 290–298.
[36] V.P. Santos, M.F.R. Pereira, J.J.M. Órfão, J.L. Figueiredo, Appl. Catal. B: Environ. 99 (2010) 353–363.
[37] K. Frey, V. Iablokov, G. Sáfrán, J. Osán, I. Sajó, R. Szukiewicz, S. Chenakin, N. Kruse, J. Catal. 287 (2012) 30–36.
[38] F. Wang, H. Dai, J. Deng, G. Bai, K. Ji, Y. Liu, Environ. Sci. Technol. 46 (2012) 4034–4041.
[39] C. Cao, Y. Zhang, D. Liu, M. Meng, Small 11 (2015) 3659–3664.
[40] C. Cao, X. Li, Y. Zha, J. Zhang, T. Hu, M. Meng, Nanoscale 8 (2016) 5857–5864.
[41] Q. Li, X. Wang, Y. Xin, Z. Zhang, Y. Zhang, C. Hao, M. Meng, L. Zheng, L. Zheng, Sci. Rep. 4 (2014) 4725.
[42] Y. Chen, G. Tian, M. Zhou, Z. Huang, C. Lu, P. Hu, J. Gao, Z. Zhang, X. Tang, Environ. Sci. Technol. 50 (2016) 5825–5831.
[43] J. Luo, Q. Zhang, A. Huang, S.L. Suib, Microporous Mesoporous Mater. 35–36 (2000) 209–217.
[44] H. Muroyama, H. Asajima, S. Hano, T. Matsui, K. Eguchi, Appl. Catal. A: Gen. 489 (2015) 235–240.
[45] E. Schweda, C. Wijstefeld, J. Straihle, J. Solid State Chem. 83 (1989) 61–68.
[46] H. Wang, S. Liu, Z. Zhao, X. Zou, M. Liu, W. Liu, X. Wu, D. Weng, Catal. Sci. Technol. 7 (2017) 2129–2139.
[47] J.A. Moulijn, F. Kapteijn, Carbon 33 (1995) 1155–1165.
[48] F. Xu, Z. Huang, P. Hu, Y. Chen, L. Zheng, J. Gao, X. Tang, Chem. Commun. 51 (2015) 9888–9891.
[49] S. Bordiga, E. Groppo, G. Agostini, J.A. van Bokhoven, C. Lamberti, Chem. Rev. 113 (2013) 1736–1850.
[50] P. Hu, Z. Huang, X. Gu, F. Xu, J. Gao, Y. Wang, Y. Chen, X. Tang, Environ. Sci. Technol. 49 (2015) 7042–7047.
[51] G. Qi, J. Xu, J. Su, J. Chen, X. Wang, F. Deng, J. Am. Chem. Soc. 135 (2013) 6762–6765.
[52] P. Legutko, P. Stelmachowski, M. Trębala, Z. Sojka, A. Kotarba, Top. Catal. 56 (2013) 489–492.
[53] P. Legutko, W. Kaspera, T. Jakubek, P. Stelmachowski, A. Kotarba, Top. Catal. 56 (2013) 745–749.
[54] P. Legutko, W. Kaspera, P. Stelmachowski, Z. Sojka, A. Kotarba, Catal. Commun. 56 (2014) 139–142.
[55] P. Legutko, T. Jakubek, W. Kaspera, P. Stelmachowski, Z. Sojka, A. Kotarba, Catal. Commun. 43 (2014) 34–37.
[56] T. Jakubek, W. Kaspera, P. Legutko, P. Stelmachowski, A. Kotarba, Catal. Commun. 71 (2015) 37–41.
[57] Q. Wang, Z. Guo, J.S. Chung, Mater. Res. Bull. 44 (2009) 1973–1977.
[58] Q. Wang, J.S. Chung, Z. Guo, Ind. Eng. Chem. Res. 50 (2011) 8384–8388.
[59] C. Lu, T. Liu, Q. Shi, Q. Li, Y. Xin, L. Zheng, Z. Zhang, Sci. Rep. 7 (2017) 3300.
[60] X. Chen, H. Wang, Z. Wu, Y. Liu, X. Weng, J. Phys. Chem. C 115 (2011) 17479–17484.
[61] H. Wang, X. Chen, X. Weng, Y. Liu, S. Gao, Z. Wu, Catal. Commun. 12 (2011) 1042–1045.
[62] M. Ogura, K. Morozumi, S.P. Elangovan, H. Tanada, H. Ando, T. Okubo, Appl. Catal. B: Environ. 77 (2008) 294–299.
[63] R. Kimura, S.P. Elangovan, M. Ogura, H. Ushiyama, T. Okubo, J. Phys. Chem. C 115 (2011) 14892–14898.
[64] K. Mizutani, K. Takizawa, H. Shimokawa, T. Suzawa, N. Ohyama, Top. Catal. 56 (2013) 473–476.
[65] C. Su, P.J. McGinn, Appl. Catal. B: Environ. 138–139 (2013) 70–78.
[66] C. Su, P.J. McGinn, Catal. Commun. 43 (2014) 1–5.
[67] J. Zokoe, P.J. McGinn, Chem. Eng. J. 262 (2015) 68–77.